Journal of Science and Technology in Civil Engineering, HUCE, 2024, 18 (2): 56–71

EXPERIMENTAL RESEARCH AND ARTIFICIAL NEURAL NETWORK-BASED PREDICTION MODEL ON COMPRESSIVE STRENGTH OF HARDENED CEMENT PASTES CONTAINING FLY ASH AND SILICA FUME AT HIGH TEMPERATURES

Do Thi Phuong[a,*], Nguyen Van Quang[a], Vuong Le Thang[b], Vu Minh Duc[c]

[a]*Faculty of Road and Bridge Engineering; The University of Danang, University of Science and Technology, No. 54 Nguyen Luong Bang road, Lien Chieu district, Da Nang city, Vietnam*
[b]*Faculty of Civil Engineering; The University of Danang, University of Science and Technology, No. 54 Nguyen Luong Bang road, Lien Chieu district, Da Nang city, Vietnam*
[c]*Faculty of Building Material; Hanoi University of Civil Engineering, No. 55 Giai Phong road, Hai Ba Trung district, Hanoi, Vietnam*

Article history:
Received 19/02/2024, Revised 30/05/2024, Accepted 11/06/2024

Abstract

The composition of the binder mixture affecting the workability of concrete at high temperatures was studied on a binder mixture of cement, fly ash, and silica fume. In this work, active mineral additives (fly ash and silica fume) were used to partially replace cement with a total substitution content of 20÷50% (fixed silica fume content with 5% and 15%). The binder samples were determined for compressive strength after being heat treated at different temperature levels from 25 to 1000 °C for 2h. The study showed that binder samples with a binder mixture composition containing 15% fly ash and 5% silica fume obtained the highest strength in the temperature range of 200÷800 °C compared to PC control samples and samples with other ratios. The samples significantly attenuated the compressive strength when exposed to more than 800 °C. In addition, this study constructed two predictive models using artificial neural networks to forecast the compressive strength based on input parameters including data on fly ash, silica fume and temperature (1); to predict the contents of fly ash and silica fume based on input parameters of compressive strength and working temperature (2). The models were built on the practical data showing the good fitting.

Keywords: fly ash; silica fume; artificial neural network; heat resistance binder; self-autoclaving process; hardened cement paste; compressive strength.

https://doi.org/10.31814/stce.huce2024-18(2)-05

1. Introduction

Concrete using Portland cement (PC) is commonly used in the construction industry today. It can be said that there have not been better alternative materials to cement concrete in the construction industry so far due to its high compressive strength, good durability, and plasticity characteristics [1]. With purpose of reducing CO_2 emissions and raising economic-environmental efficiency, mineral admixtures such as fly ash, blast furnace slag, silica fume are now used in concrete to partially replace cement for high-strength concrete production. Although these types of concrete have low thermal conductivity and high specific heat, they are still greatly affected under the high temperature of the fire [2, 3]. The mechanical properties of concrete or mortar including strength, elasticity and volume expansion, concrete density, and color appearance change significantly under high flame temperatures, resulting in deterioration of concrete quality and undesirable structural failures, especially in concrete

*Corresponding author. *E-mail address:* dtphuong@dut.udn.vn (Phuong, D. T.)

structures working in industrial production furnaces or reactors [4]. The high-performance concrete and normal concrete show different behavior on strength loss and explosive spalling phenomena due to internal pressure or expansion of hardened cement paste under the various range of the high temperatures [1, 5]. The behavior of concrete under elevated temperatures is highly dependent on the properties of binder materials, aggregates, cement paste, cement paste-aggregate interconnection and thermal compatibility of matrix components [4]. The dehydration of hardened cement pastes as well as the decomposition of hydration minerals at high temperatures are major causes of high-temperature destruction of concrete structures. The free water decreases at below 105 °C. There is a dehydration in the gel structure of C-S-H, ettringte mineral, and gypsum up to 250 °C [6]. This is followed by dehydration of $Ca(OH)_2$ to produce CaO at the temperature range of 400÷600 °C. Moreover, the formation of CaO was also from the decomposition of $CaCO_3$ and C-S-H minerals at higher temperatures. Thus, it is the second hydrolysis of CaO that results in volume expansion, destroys the hardened cement pastes structures and weakens concrete strength [6–8]. It is important to have in-depth studies to understand the behavior of concrete under high temperatures. Currently, there have large number of research works using active mineral additives such as fly ash (FA), finely ground blast furnace slag (GGBFS), silica fume (SF), finely ground pumice (FGP), metakaolin in concrete to increase the mechanical properties and workability of concrete when working under high temperatures [1, 4, 9–12]. Bahar et al. used a combination of cement, FGP and SF with the ratio of cement: FGP: SF = 17:1:5 to fabricate heat-resistant concrete with the highest strength of 56.43 MPa at 400 °C [4]. Meanwhile, Chan et al. fabricated high-performance concrete (HPC) concrete with binder composition using FA and SF with/without using steel fibers with sizable strength attenuation of 25.6% and 34.1% before and after exposure to 800 °C [9]. Using FA and metakaolin with different proportions to produce the HPC used at different temperature levels, Abid et al. suggested that all mix proportions with FA (5÷20%) and metakaolin (20÷60%) have strength and durability loss at 400 °C and above [11]. Semsi et al. partially replaced cement with a single component of FA or SF or Pumice in mortar mixtures. The results found that the compressive strength of all mortar samples containing pozzolanic additives were less effected under high temperatures compared to control sample [10]. Donatello et al. showed that cement pastes using FA have significant differences on shrinkage and increased strength contracting to control paste without using FA under heat exposure of the above 700 °C [13]. Additionally, Rahel et al. fabricated fire resistance mortar using high-volume FA and colloidal silica nano with higher strength properties at high temperatures 400÷700 °C compared to control [14]. Hekal et al. reported the hardened cement paste made from 10%SF and 10%FA performed the good fire resistance up to 450 °C [15]. It can be seen that the research on behaviors of heat resistance binder or hardened cement paste using the combination between SF and FA under high temperatures have some limitations such as less number of research and working temperatures up to 1000 °C not being done.

On the other hands, the experiments on concrete or mortars require a massive number of work-loading because their strength characteristics strongly depend on variables or parameters such as types of binder, water/binder ratios, fine aggregates, coarse aggregates, curing conditions, mixing methods [16]. The construction of prediction models for high accuracy is necessary not only to reduce work loading in experiments but also determine optimal mixtures with designed compressive strength [17]. Recently, artificial neural networks and multivariate regression models were commonly applied on prediction of compressive strength. The multivariate regression models have some drawbacks due to low accuracy when taking account of the large number of input variables and the interaction among variables [17, 18]. However, artificial neural network models have been considered as a dominant choice to solve complicated problems with the assistance of computational elements. With its benefits,

artificial neural networks (ANNs) models was widely applied in many aspects of today's construction technology including concrete durability, shrinkage, slump model, concrete workability, concrete properties under high temperatures, and compressive strength behavior of concrete containing fly ash and silica fume [19].

The binder mixtures in this study include cement, fly ash, and silica fume, in which the total cement-substitution content of 20 to 50%, fixed silica fume contents of 5% and 15% were employed to investigate the compressive strength behaviors under elevated temperatures. Additionally, an ANN model was constructed to predict the compressive strength of hardened cement paste samples using FA and SF as partial substitution of cement at elevated temperatures up to 1000 °C. The ANN model takes FA/binder and SF/binder ratios and temperature as inputs to predict the compressive strength of hardened cement paste samples. The number of samples required for the experiment depends on the chosen experimental design method. Additionally, a separate ANN model is built with compressive strength and temperature as inputs, while the outputs are the two-component quantities (fly ash and silica fume) needed to achieve the desired strength and temperature requirements.

2. Experimental procedure

2.1. Materials

PC50 Song Gianh cement (Vietnam) used in the study has properties satisfying TCVN 2682: 2020 [20]. The 28-day age compressive strength of cement is 51.9 MPa. Fly ash (FA) and silica fume (SF) are used as active mineral additives in the binders. The FA (Class F) with a particle size of ≤ 0.09 mm in the study is waste product of Vinh Tan thermal power plant (Vietnam). The SF under powder form is a waste product from the production process of silicon or ferro-silicon alloy, supplied by Sika company. The active mineral additives have properties satisfying TCVN 10302:2014 [21] and TCVN 8827:2011 [22]. The strength activity index of FA and SF is 89.8% and 109.2%, respectively. The surface area of PC is 3810 cm^2/g, whereas that of SF and FA are 176600 cm^2/g and 3550 cm^2/g respectively. Some of the physical properties and chemical composition of PC cement and active mineral additives are shown in Table 1.

Table 1. Properties of Portland cement and active mineral additives

Properties	Cement	FA	SF
Chemical composition, %			
SiO_2	21.09	55.20	90.26
Al_2O_3	6.53	20.97	1.05
Fe_2O_3	3.34	6.27	1.03
CaO	64.21	0.95	1.23
MgO	0.85	1.54	1.41
Na_2O	-	0.54	0.91
K_2O	2.91	3.39	2.03
SO_3	0.15	0.13	0.02
Loss on ignition (LOI)	0.83	11.00	2.03
Physical properties			
Specific gravity, g/cm^3	3.11	2.29	2.22
Bulk density, kg/m^3	973	982	699

2.2. *Mix proportions*

Binder samples containing PC cement, FA and SF are prepared. The total content of active mineral additives including FA and SF replace 20÷50% of cement (in weight, wt.%), in which FA is used replacing 15%, 25% and 35% while SF is substituted by 5% and 15%. The water used in the study is the standard water amount of the binder mixture. Details of mix proportions are shown in Table 2.

Table 2. Mix proportions of specimens, wt.%

Sample no.	Cement	FA	SF	Standard Water
PC	100	0	0	32.0
FA15SF5	80	15	5	31.0
FA25SF5	70	25	5	30.0
FA35SF5	60	35	5	29.5
FA15SF15	70	15	15	31.5
FA25SF15	60	25	15	30.5
FA35SF15	50	35	15	30.2

2.3. *Casting, curing, and testing of specimens*

Samples are cast by using a 2 × 2 × 2 cm mold [12, 23]. The samples were cured in conditions of temperature of 27 ± 2 °C, humidity not less than 95% for 20 hours and steam curing at 100 °C for 4 hours. Next, the sample is dried at 100 °C until a constant mass of sample and then heated at

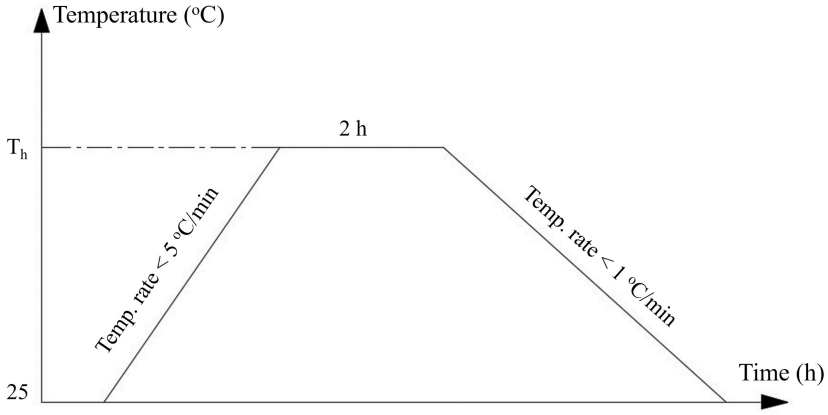

Figure 1. The thermal processing line of hardened cement pastes (Th: the highest temperature)

(a) Casting (b) Curing (c) Elevated temperature (d) Compressive strength test

Figure 2. Experimental process

temperature levels of 200, 400, 600, 800, and 1000 °C and keep at each temperature level for 2 hours. The temperature ramping rate is less than 5 °C/min. The graph of the firing curve of binder samples is shown in Fig. 1. The sample is cooled to room temperature with temperature rate of less than 1 °C/min and then the compressive strength was measured. Pictures of the experimental process are shown in Fig. 2. The XRD and SEM analysis of samples is also shown in the paper.

3. Experimental results and discussions

3.1. Compressive strength of hardened cement samples at high temperatures

The results of compressive strength of binder samples made with PC, FA, and SF at various temperatures in Fig. 3. The compressive strength of the samples increases when heated to 200 °C and decreases when heated to 1000 °C.

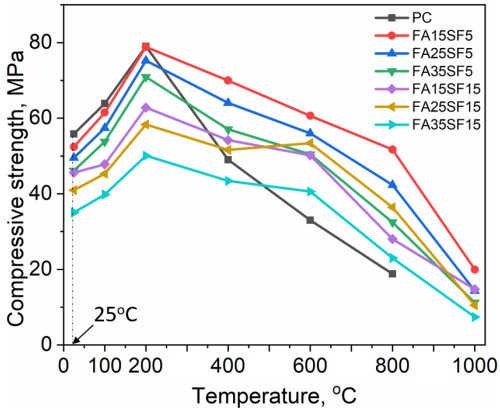

Figure 3. Compressive strength of hardened cement pastes samples at different temperature levels

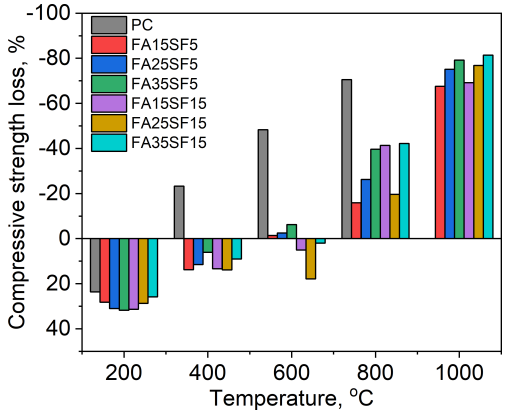

Figure 4. The compressive strength of hardened cement pastes samples at temperature levels in comparison with the samples at 100 °C, %

The PC sample had an increase by 23.7% in the compressive strength value at 200 °C compared to that of the heated sample at 100 °C (Fig. 4). At high temperatures, water loss is accompanied by strong shrinkage and increase in the density in the sample, while the free water separation promotes the hydration of cement increasing the strength (self-autoclaving process) [24]. When heating the sample to 400 °C, compressive strength of the PC sample decreased by 23.3% compared to its strength at 100 °C due to the dehydration of mainly C-S-H mineral, ettringite, a decomposition of $CaSO_4 \cdot 2\,H_2O$ [6, 7]. At 600 °C, the compressive strength of the PC sample plummeted by 48.3% compared to that of temperature-treated sample at 100 °C, which results from the decomposition of $Ca(OH)_2$ into free CaO and the occurrence of hydration reactions when encountered moisture in the pores producing the micro-cracks [8, 24]. At 800 °C, the compressive strength of the PC sample loses 70.6% compared to the compressive strength of sample at 100 °C and they were completely destroyed when heated to 1000 °C. The decomposition of C-S-H mineral and $CaCO_3$ occurring at this stage is also responsible for strength loss [7, 23, 25]. Some authors pointed out that PC cement based samples were completely destroyed at 800 °C [15].

For samples containing FA and SF, the strength value increased from 25.8÷31.8% when heated to 200 °C. The increase in compressive strength at this temperature is partly due to the "self-autoclaving process", partly due to the reaction of CH with the active mineral additives in binder mixtures that increases the initial strength [24, 26, 27]. Meanwhile, studying on PC cement samples working at 25÷800 °C, M. Heikal et al. [15] suggested that the compressive strength was the highest at approximately 450 °C for samples containing FA and SF. H. El-Didamony [28] concluded that cement based

samples containing FA and fired clay bricks obtained the highest compressive strength at 250 °C. In the calcining process of cement samples from a very high volume fly ash cement paste, the results of S. Donatello's research showed that residual compressive strengths increased by around 100% at temperatures more than 600 °C [13].

The compressive strength of the samples also decreased when heated from 200÷1000 °C but the compressive strength reduction was lower than that of PC samples. At about 200÷400 °C, the samples had compressive strength 1.1÷1.4 times higher than the PC sample and increased by 6.1÷13.9% compared to that of treated sample at 100 °C. Active mineral additives increased the filling effect and the reaction between the active SiO_2 and components of the mineral additives with CH components in hardened cement paste produced the C-S-H, C-A-H, C-A-S-H minerals [15, 26, 29–31]. These new minerals have a certain stability as well as tighten the structure of the hardened cement pastes. Those are responsible for increasing the strength of the samples. According to some authors about those samples, there are hydration products consisting of tobermorite mineral ($5\,CaO \cdot 6\,SiO_2 \cdot xH_2O$), which are 2 to 3 times more stable than C-S-H mineral [26, 32]. Continuing to increase the temperature, the compressive strength of samples containing active mineral additives is 1.2 to 1.8 times higher at 600 °C and 1.2 to 2.8 times higher at 800 °C than that of the sample at 100 °C. The free CaO component produced in hardened cement paste may have been eliminated due to occurrence of pozzolanic reaction, particularly with the appearance of SF. Heating up to 1000 °C, samples containing mineral additives decreased markedly, losing strength by 67.5÷81.4% compared to that of the sample at 100 °C.

The compressive strength value of samples containing mineral additives at each temperature level depends on the content of mineral additives. For the sample group containing 15% SF, the FA25SF15 sample had the highest strength at about 600÷800 °C of 53.4 MPa (at 600 °C) and 36.4 MPa (at 800 °C) but decrease when heated to 1000 °C. For the sample group containing 5% SF, the FA15SF5 sample obtained a compressive strength of 51.7 MPa at 800 °C, a loss of 15.7% compared to that of the sample at 100 °C. Meanwhile, the author M.Heikal [15] showed that the cement sample containing 15% FA and 5% SF had compressive strength at 800 °C losing 15% compared to that of sample at 25 °C. However, up to 1000 °C, the compressive strength of the sample FA15SF5 was only 14.7 MPa, sinking by 67.5% compared to that of the sample at 100 °C. Thus, the temperature for the best working ability of samples containing mineral additives is less than 800 °C.

The next study demonstrates the results of XRD and SEM analysis of the FA15SF5 sample at temperature levels to show the relationship between physicochemical changes and compressive strength of samples at high temperatures.

3.2. XRD Analysis

X-ray diffraction analysis (XRD) is a technique used in materials science to determine the crystallographic structure of a material in the hydration products of sample in the presence of FA and SF at elevated temperatures. Fig. 5 shows the results of XRD analysis of FA15SF5 samples at normal temperature and after treated at 100, 200, 400, 600, 800, and 1000 °C. At a temperature of 25 °C, the CH mineral appears with a strong intensity of the peaks at 17.9°, 29.2°, 34.5°, 47.3°, and 51.8° 2θ. The presence of C_2S mineral was detemined by characteristic peak at 2θ of 32.1° while the C_3S mineral had the peaks at 32.2° and 41.3° 2θ. The peak of $CaCO_3$ mineral was at 2θ of 29.7°. The C-S-H mineral was detected from XRD pattern by the peaks at 29.0°, 28.9°, 31.8°, and 49.4° 2θ.

The interaction of FA and SF with $Ca(OH)_2$ of hardened cement pastes to produce C-S-H, C-A-S-H minerals [15, 30, 31]. That was proved for the existance of the C_2ASH_8 mineral which was

detected when the sample was heated at 200 °C but with a low intensity of the peak at 2θ of 42.6°. The β-C_2S, C_3S, $CaCO_3$, CS, and C_2AS minerals appeared in the sample at 800 °C.

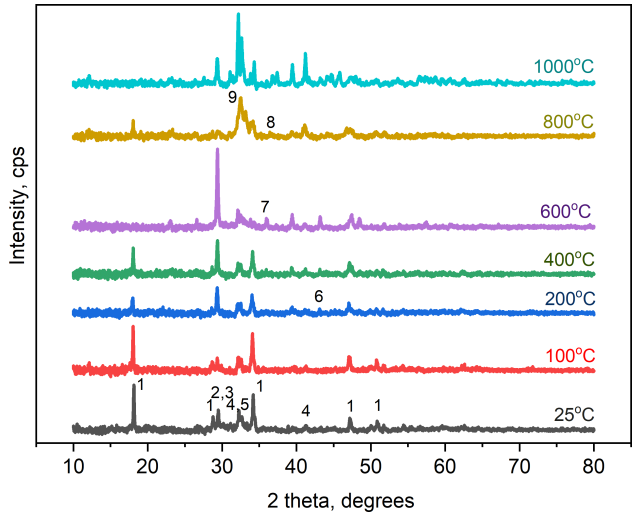

Figure 5. Results of XRD analysis of FA15SF5 samples at temperature levels.
(1- CH; 2- $CaCO_3$; 3- C-S-H; 4- C_3S; 5- C_2S; 6- C_2ASH_8; 7- CaO; 8- CS; 9- C_2AS)

The decomposition of C-S-H, C-A-S-H minerals at high temperatures is the basis for the formation of new minerals, namely CS and C_2AS crystals. The appearance of CS mineral is characterized by the peaks at 31.8°, 32.1°, and 36.6° 2θ. The C_2AS mineral was detected with the peaks at 32.1° and 53.4° 2θ for samples treated at 800 °C. The XRD analysis of samples at 1000 °C demonstrated the existence of these minerals with higher intensity. A further observation showed the existence of the CS mineral by the peaks at 27.7°, 45.8° 2θ and C_2AS mineral with higher intensity of peaks at 24.6°, 32.1°, and 53.4° 2θ. The CS mineral also appeared at 800 °C with binder samples containing 20% SF in the study by the author [15]. The presence of CS and C_2AS minerals are responsible for the structural stability of the FA15SF5 sample at about 800 °C, reducing the loss in compressive strength. It also confirms the further formation of C-S-H and C-A-S-H minerals occurs from the reaction between the compositions of the mineral additives FA, SF, and hardened cement paste. In particular, the PC sample at 1000 °C was completely destroyed. The structure of CS, C_2AS minerals stabilized in the hardened cement pastes samples reduced the loss of the compressive strength. Therefore, the strength of the FA15SF5 sample was still 19.97 MPa.

The peak intensity of the CH decreases and the peak intensity of C-S-H increases markedly with an increase in temperature of from 200 to 600 °C. This demonstrates the conversion of CH to C-S-H due to the reaction with active mineral additives. The tobermorite mineral formed at about 200÷400 °C in the sample of hardened cement paste containing FA and at about 500 °C in the sample containing blast furnace slag, SF and fired clay brick powder [23, 26, 32]. The transition of C-S-H phases to tobermorite phase formed a high-strength product. This may be one of the reasons to explain for the higher compressive strength of samples containing FA and SF than that of high-temperature treated PC control samples. However, peak intensity of the C-S-H was quite low and almost disappeared for the FA15SF5 sample at around 800 °C. Some other studies suggested that hardened cement paste samples containing some active mineral additives occurred the decomposition of C-S-H at about 800 °C, but there are also other studies showed that C-S-H mineral such as tobermorite convert to CS mineral or larnite crystals when heated to 900 °C [15, 23, 33].

3.3. SEM analysis

The results of SEM analysis on FA15SF5 samples at temperature levels are shown in Fig. 6. Hexagonal lamellar CH crystals and filamentous C-S-H crystals in the SEM image of the sample at 25 °C were observed (Fig. 6(a)). Hydration process is promoted so that CH crystals are more abundantly observed in Fig. 6(b) under blocks arranged parallel and thin plates parallel in Fig. 6(c). The filamentous C-S-H mineral are alternately distributed between CH blocks in the SEM of treated samples at 100 °C and 200 °C (Fig. 6(b) and 6(c)), and under the form of tight interconnection in the sample treated at 400 °C (Fig. 6(d)) and in the form of small rods in sample calcined at 600 °C (Fig. 6(e)) [23, 28]. The reaction between the hydration products of cement and mineral additives produced the C-S-H mineral as confirmed in the XRD study. The formation of this C-S-H mineral has increased the density of hardened cement samples and their compressive strength increased by 28.2% at 200 °C, 13.8% at 400 °C, and only loss by 1.4% at 600 °C. The SEM image of FA15SF5 sample calcined at 800 °C appeared new small needle-shaped crystals distributed alternately in glass phases (Fig. 6(f)) and this clearly showed in SEM images of the treated sample at 1000 °C (Fig. 6(g)). Thus, the existence of new minerals is in agreement with the results of XRD data and the structure is improved in comparison with the PC sample, indicating that the decrease in compressive strength is lower than that of the PC sample. At the temperature range of 800÷1000 °C, the structure of the hardened cement paste changes to the structure of ceramic materials including phases: crystalline phase;

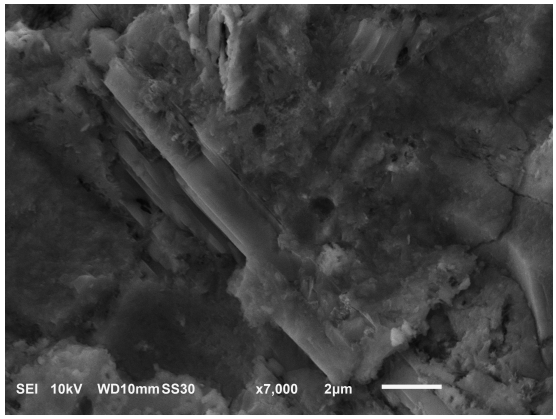

(a) At 25 °C

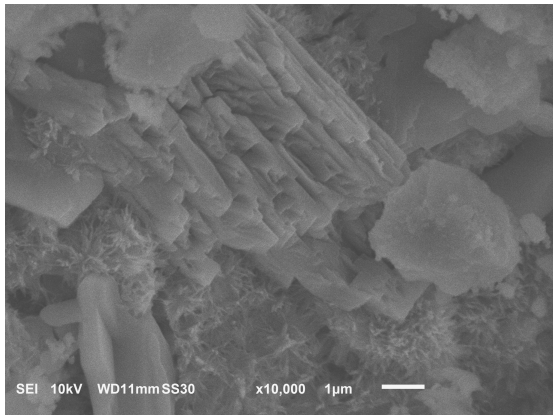

(b) At 100 °C

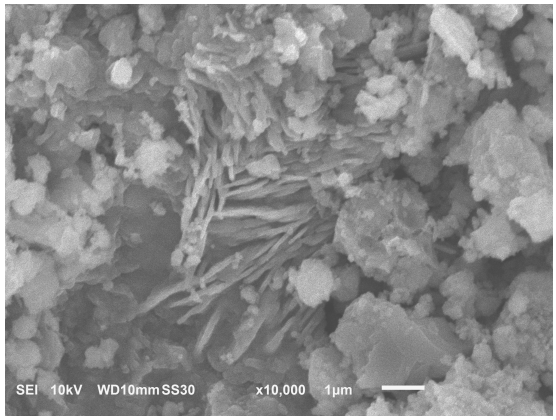

(c) At 200 °C

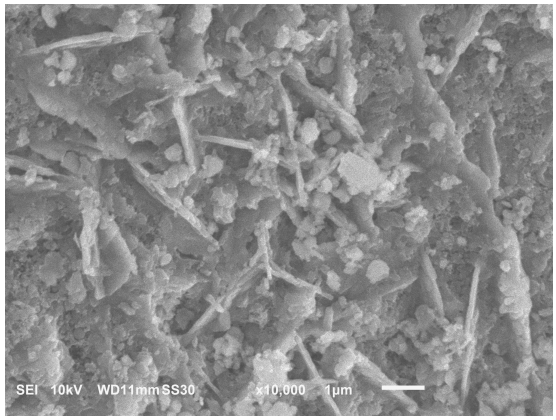

(d) At 400 °C

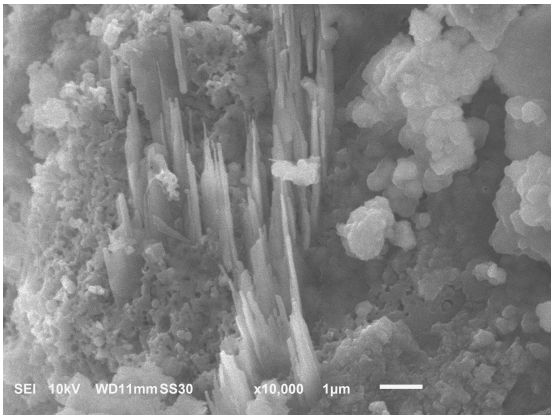

(e) At 600 °C

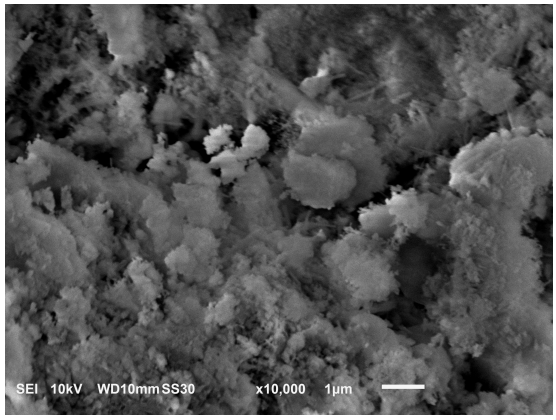

(f) At 800 °C

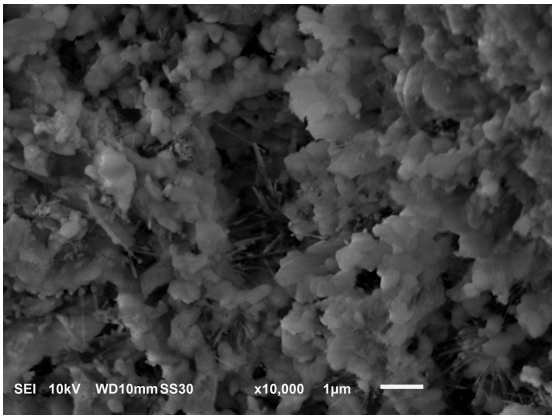

(g) At 1000 °C

Figure 6. SEM analysis results of FA15SF5 samples at temperature levels

glass phase (silicate melting agents) and pore system (cracks, closed pores, openings, microscopic, and so on). The pore system observed in the SEM images could explain the decrease in the samples' compressive strength at this temperature range compared to the range of 100-600 °C.

3.4. Application of artificial neural network modeling in predicting compressive strength and hardened cement paste composition

An artificial neural network (ANN) model is constructed to predict the compressive strength of hardened cement paste with the change of two mineral additives FA and SF at temperature ranges varying from 25 to 1000 °C. An urgent practical requirement to prepare binder mixture is to find out FA and SF ratios to replace PC cement, which meets the required compressive strength and temperature.

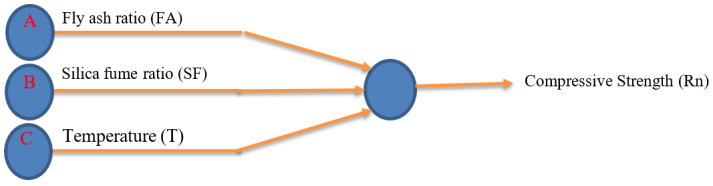

Figure 7. The model predicts the compressive strength of hardened cement paste

Thus, another ANN network is built to predict the compositions of FA and SF to meet the required compressive strength and temperature. The input and output parameters of the compressive strength prediction model are shown as Fig. 7 and the FA and SF content prediction model are shown as Fig. 8.

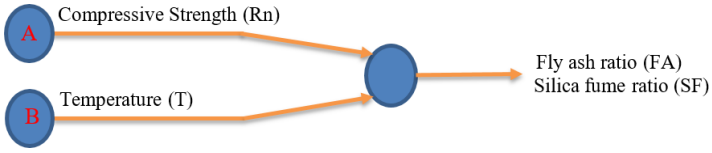

Figure 8. FA and SF content prediction model

a. Construction of a predictive model

- Datasets serving the ANN network

The study was conducted to replace cement by FA with three percentage of 15%, 25% and 35%; the proportion of SF replacing cement with two percentages of 5% and 15%; The seven level temperatures change are 25, 100, 200, 400, 600, 800, and 1000 °C. Using a full factorial experimental planning method, the amount of data used for ANN network training was determined: Number of data = 21 × 31 × 71 = 42 data. Interpretation of the variability of the three input parameters is shown as Table 3 and the compressive strength of the samples shown in Fig. 4.

Table 3. Interpretation of the input dataset of the predictive model

Label	Parameters (unit)	Level of variation							Number of levels
		1	2	3	4	5	6	7	
A	FA (%)	15	25	35	*	*	*	*	3
B	SF (%)	5	15	*	*	*	*	*	2
C	T (°C)	25	100	200	400	600	800	1000	7

- Predictive model structure

The pairing structure between neurons into networks will directly affect operational efficiency as well as on the processes of determining and adapting pairing weights. In this study, the MultiLayer Perceptron (MLP) network model with a hidden layer was used as shown in Fig. 9, where the network has N inputs, M neurons on the hidden layer, and K outputs [34].

When one structure with a given number of hidden neurons is trained to match one set of learning samples, the neuronal connection weighting is adjusted. The symbol for the metric sample set consists of p pairs of the input-output corresponding to $\{x_i, d_i\}$, with $i = 1, ..., p$; $x_i \in \mathbb{R}^N$; $d_i \in \mathbb{R}^K$; MLP parameters are adjusted so that the error function has the smallest value:

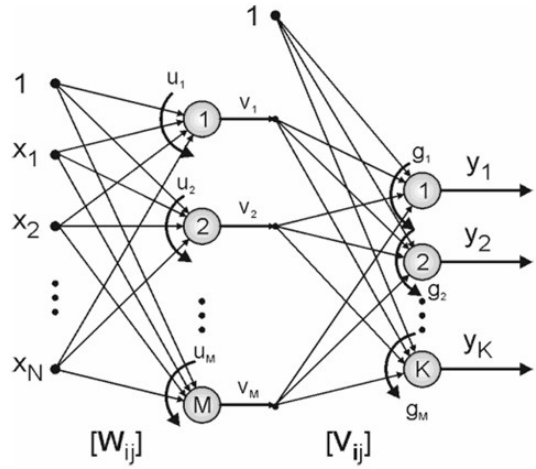

Figure 9. The MLP network structure with one input layer, one hidden layer, and one output layer [34]

$$E = \frac{1}{2}\sum_{i=1}^{p} \|MLP(x_i) - d_i\|^2 \rightarrow \min$$

where E is an error function.

The ANN network structure in the study consists of three layers: the input layer, the hidden layer, and the output layer. The two ANN models are constructed with the input layer of input parameters and the output layer of the output parameters, respectively, as shown in Fig. 7 and Fig. 8. The hidden layer consists of two parameters, the number of hidden layers and the number of neurons in the hidden layers, and the change of these parameters will affect the accuracy of the prediction model. The work uses a trial-and-error method to find the most suitable ANN network structure. Then a hidden layer with 15 neurons is selected and the structure of the two ANN networks is shown as Fig. 10 and Fig. 11. The used training function is Levenberg Marquardt (TRAINLM), the used activation function (transmission function) is TANSIG.

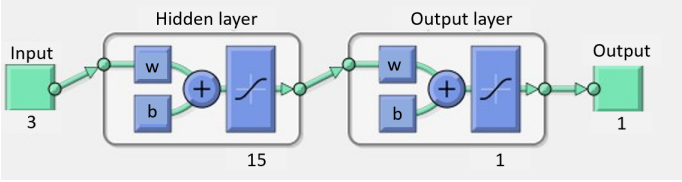

Figure 10. The ANN1 network structure is used for cement compressive strength prediction

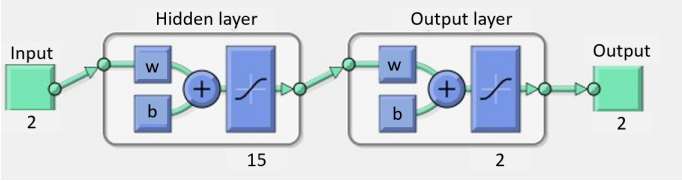

Figure 11. The ANN2 network structure is used for the prediction of content FA and SF

A total of 42 experimental datasets were used for training, validation, and testing. The used data were 70% (30 samples), 15% (6 samples), and 15% (6 samples) for training, validation, and testing, respectively. The allocation of 42 datasets to the above three datasets was done randomly using the tool in MATLAB software.

- Evaluation parameters

In this study, the R-factor was used to assess the relevance of the analytical model to empirical data. The coefficient R is determined by Eq. (1).

$$R = \sqrt{1 - \frac{\sum_{i=1}^{n} (y_i - \hat{y}_i)^2}{\sum_{i=1}^{n} (y_i - \bar{y}_i)^2}} \tag{1}$$

where y_i is the output variable value of experiment i; $\hat{y}_i$ is the predicted value of the output variable of the experiment (i); $\bar{y}$ is the average value of the output variable of all experiments; and n is the number of tested samples.

b. Predicted results and discussions

- Prediction of hardened cement paste compressive strength

The results of ANN1 network training to predict compressive strength of hardened cement paste are shown in Fig. 12 where the vertical axis is the mean squared error (MSE) and the horizontal axis is the number of training iterations. The training process shows that the lines of training, validation and testing are similar. The best validation performance with an MSE index of 24.5699 at the 19th loop, after which the training continued until the 25th loop stopped. Moreover, the training process showed no recorded overfitting.

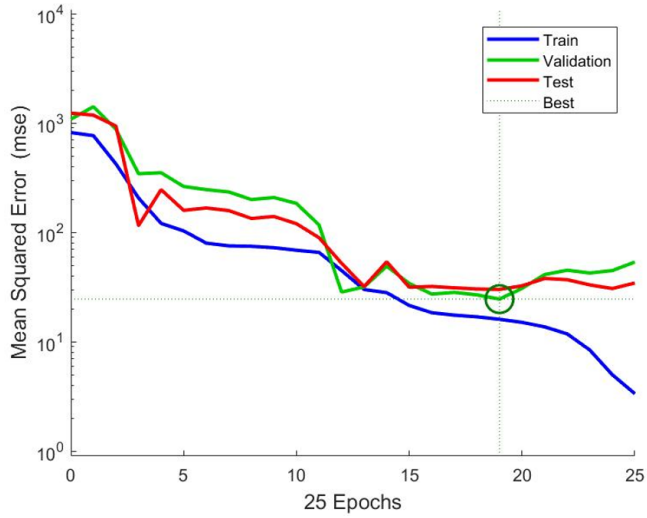

Figure 12. The training process predicts the compressive strength of hardened cement paste at high temperatures

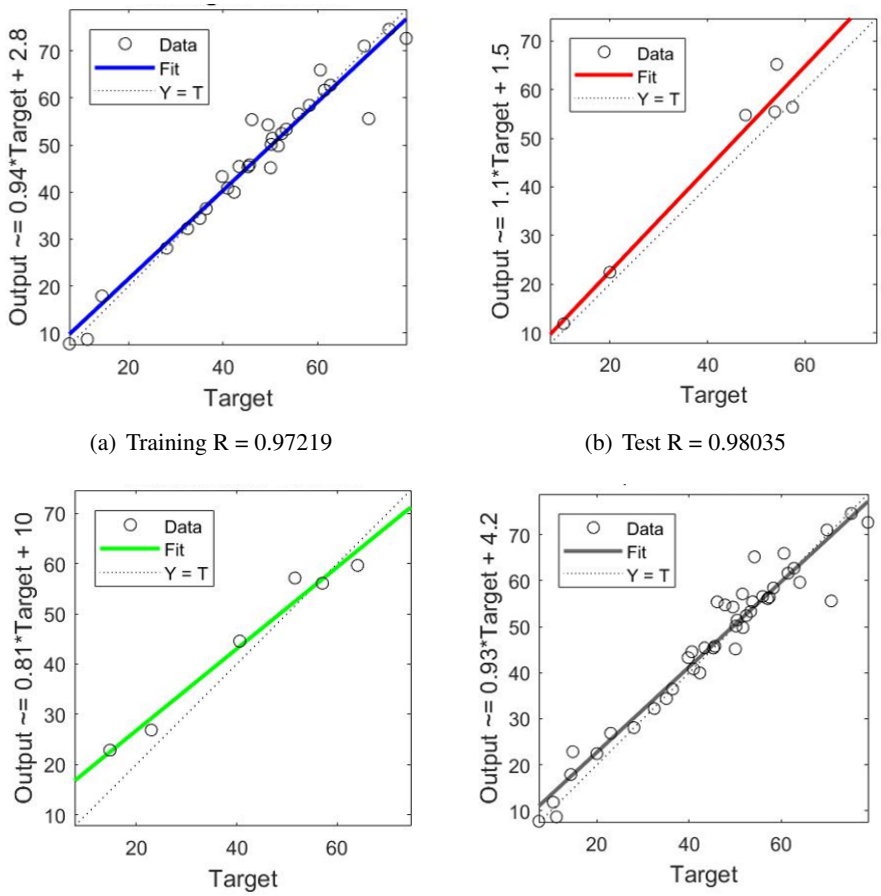

(a) Training R = 0.97219

(b) Test R = 0.98035

(c) Validation R = 0.98537

(d) All R = 0.96973

Figure 13. The results predict the compressive strength of hardened cement paste at high temperatures

Fig. 13 shows the relationship between the output of the network and the targets. The three charts represent training, validation, and testing data. The dashed line in each chart demonstrated the perfect results when the output is equal to the target.

The solid line represents the most suitable linear regression line between the output and the target. The predicted compressive strength (output) relative to the experimental results (target) of all three models has a good fitting. At the same time, the approximating line predicted compressive strength for both cases coincides with the line Y = T of the graph. With the above forecasting model structure, the results showed that artificial neural network models are highly accurate (R = 0.96973).

- Prediction on FA and SF content to meet temperature requirements and compressive strength

The results of ANN2 network training to predict FA and SF content (%wt, vs. binders) to meet working temperature requirements and compressive strength are shown in Fig. 14. The MSE's best validation performance was 10.5045 at the 16th loop, after which the training continued until the 36th loop stopped. Like the ANN1 model, the training showed no overfitting. The training, evaluation, and testing process are shown in Fig. 15 and the evaluation coefficient of the model is R = 0.88067. This result is not too good, but it is also at a level meeting the requirements. Three examples of predicted results on FA and SF content meeting the required compressive strength and temperature requirements are shown in Table 4.

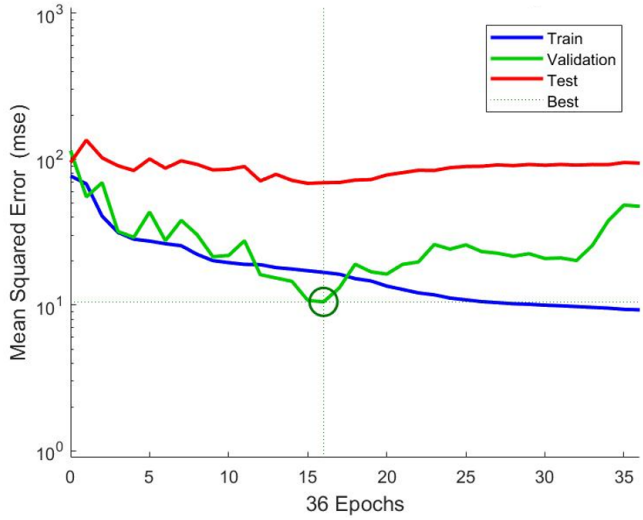

Figure 14. The training predicts FA and SF content to meet compressive strength and working temperature

Table 4. Prediction of FA and SF content to meet compressive strength and working temperature

No	Required R_c (MPa)	Required T (°C)	Predictive modeling	Predicted results	
				FA (%)	SF (%)
1	40	800	ANN2	26.7830	10.3081
2	30	800	ANN2	34.9839	13.0386
3	50	800	ANN2	15.0026	5.0013

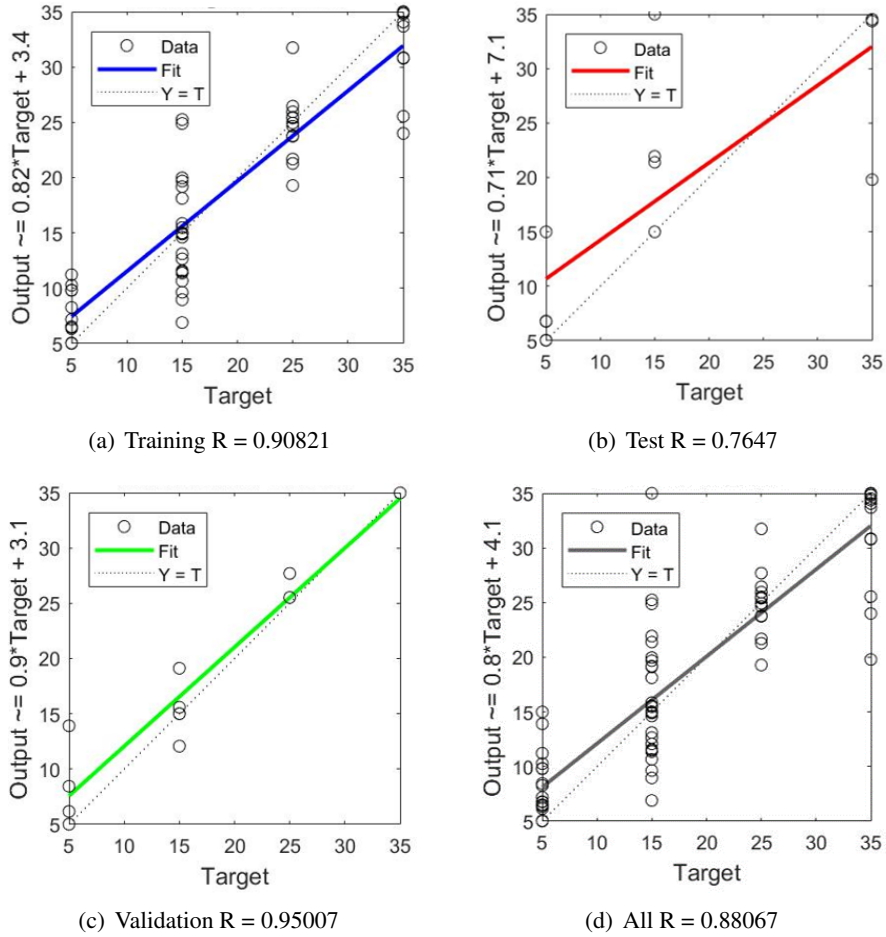

(a) Training R = 0.90821

(b) Test R = 0.7647

(c) Validation R = 0.95007

(d) All R = 0.88067

Figure 15. The predicted results of FA and SF content meeting the compressive strength of hardened cement paste and at the required temperature

4. Conclusions

Some of the conclusions from the study are as follows:

- All samples surveyed in this study tended to increase compressive strength when heated to 200 °C. The PC control sample significantly reduced its strength when exposing to more than 200 °C and lost 70.6% of its compressive strength at 800 °C, completely destroyed when reaching greater than 800 °C.

- Active mineral additives of FA and SF replacing PC cement can improve the compressive strength of hardened cement paste at high temperatures, especially at temperatures less than 800 °C. The sample contains 15%FA and 5%SF for the highest compressive strength, the compressive strength of the sample at 800 °C is reduced by 15.7%.

- The C-S-H and C-A-S-H minerals are generated in the temperature range of 200÷600 °C, followed by the formation of minerals CS ($CaSiO_3$), C_2AS ($Ca_2Al(AlSiO_7)$) at 800÷1000 °C. These formed minerals confirm the chemical interactions among SiO_2, Al_2O_3, and CaO components of FA, SF, and hardened cement paste, leading the reduction of free CaO content and the increase in compressive strength.

- The ANN1 model accurately predicts the compressive strength of hardened cement pastes within

the range of 7.39 MPa to 78.86 MPa when using FA (1%÷35%) and SF (5%÷15%) as partial cement substitutes, at temperatures ranging from 25 °C to 1000 °C (R-value: 0.96973). Meanwhile, the ANN2 model, given desired compressive strength and temperature settings, recommends the optimal FA and SF quantities to achieve them (R-value: 0.88067).

Acknowledgements

The authors sincerely thank to the financial support of The University of Danang, University of Science and Technology, code number of Project: T2023-02-43.

References

[1] Kim, G.-Y., Kim, Y.-S., Lee, T.-G. (2009). Mechanical properties of high-strength concrete subjected to high temperature by stressed test. *Transactions of Nonferrous Metals Society of China*, 19:s128–s133.

[2] Chee Ban, C., Sern, L. J., Jasme, N. (2019). The mechanical strength and drying shrinkage behavior of high performance concrete with blended mineral admixture. *Jurnal Teknologi*, 81(4).

[3] Morsy, M. S., Alsayed, S. H., Aqel, M. (2010). Effect of elevated temperature on mechanical properties and microstructure of silica flour concrete. *International Journal of Civil & Environmental Engineering*, 10(1):1–6.

[4] Demirel, B., Keleştemur, O. (2010). Effect of elevated temperature on the mechanical properties of concrete produced with finely ground pumice and silica fume. *Fire Safety Journal*, 45(6–8):385–391.

[5] Husem, M. (2006). The effects of high temperature on compressive and flexural strengths of ordinary and high-performance concrete. *Fire Safety Journal*, 41(2):155–163.

[6] Bažant, Z. P., Kaplan, M. F. (2018). Concrete at high temperatures: material properties and mathematical models. *(No Title)*.

[7] Hager, I. (2013). Behaviour of cement concrete at high temperature. *Bulletin of the Polish Academy of Sciences: Technical Sciences*, 61(1):145–154.

[8] Remnev, V. V. (1996). Heat-resistant properties of cement stone with finely milled refractory additives. *Refractories*, 37(5):151–152.

[9] Chan, Y. N., Luo, X., Sun, W. (2000). Compressive strength and pore structure of high-performance concrete after exposure to high temperature up to 800°C. *Cement and Concrete Research*, 30(2):247–251.

[10] Yazıcı, Ş., Sezer, G. İ., Şengül, H. (2012). The effect of high temperature on the compressive strength of mortars. *Construction and Building Materials*, 35:97–100.

[11] Nadeem, A., Memon, S. A., Lo, T. Y. (2014). The performance of Fly ash and Metakaolin concrete at elevated temperatures. *Construction and Building Materials*, 62:67–76.

[12] Do, T. P., Nguyen, V. Q., Vu, M. D. (2020). A Study on Property Improvement of Cement Pastes Containing Fly Ash and Silica Fume After Treated at High Temperature. In *Computational Intelligence Methods for Green Technology and Sustainable Development*, Springer International Publishing, 532–542.

[13] Donatello, S., Kuenzel, C., Palomo, A., Fernández-Jiménez, A. (2014). High temperature resistance of a very high volume fly ash cement paste. *Cement and Concrete Composites*, 45:234–242.

[14] Ibrahim, R. K., Hamid, R., Taha, M. R. (2012). Fire resistance of high-volume fly ash mortars with nanosilica addition. *Construction and Building Materials*, 36:779–786.

[15] Heikal, M., El-Didamony, H., Sokkary, T. M., Ahmed, I. A. (2013). Behavior of composite cement pastes containing microsilica and fly ash at elevated temperature. *Construction and Building Materials*, 38: 1180–1190.

[16] Thang, V. L., Cung, L., Son, N. D. (2022). An Application of Artificial Neural Network to Predict the Compressive Strength of Concrete using Fly Ash and Stone Powder Waste Products in Central Vietnam. *International Journal of Engineering*, 35(5):967–976.

[17] Thang, V. L., Cung, L., Son, N. D. (2024). Predicting Concrete Slump using Fly Ash and Stone Powder in Central Vietnam. *Tehnicki vjesnik - Technical Gazette*, 31(1):79–87.

[18] Chandwani, V., Agrawal, V., Nagar, R. (2015). Modeling slump of ready mix concrete using genetic algorithms assisted training of Artificial Neural Networks. *Expert Systems with Applications*, 42(2):885–893.

[19] Uysal, M., Tanyildizi, H. (2012). Estimation of compressive strength of self compacting concrete containing polypropylene fiber and mineral additives exposed to high temperature using artificial neural network. *Construction and Building Materials*, 27(1):404–414.
[20] TCVN 2682:2020. *Portland cements*. Ministry of Science and Technology.
[21] TCVN 10302:2014. *Activity admixture-Fly ash for concrete, mortar and cement*. Ministry of Science and Technology.
[22] TCVN 8827:2011. *Highly activity puzzolanic admixtures for concrete and mortar-Silicafume and rice husk ash*. Ministry of Science and Technology.
[23] Heikal, M. (2008). Effect of elevated temperature on the physico-mechanical and microstructural properties of blended cement pastes. *Building Research Journal*, 56(2):157–172.
[24] Morsy, M. S., Al-Salloum, Y. A., Abbas, H., Alsayed, S. H. (2012). Behavior of blended cement mortars containing nano-metakaolin at elevated temperatures. *Construction and Building Materials*, 35:900–905.
[25] Klieger, P., Lamond, J. (1994). *Significance of Tests and Properties of Concrete and Concrete-Making Materials*. ASTM International.
[26] Rashad, A. M. (2015). An investigation of high-volume fly ash concrete blended with slag subjected to elevated temperatures. *Journal of Cleaner Production*, 93:47–55.
[27] Heikal, M. (2006). Effect of temperature on the structure and strength properties of cement pastes containing fly ash alone or in combination with limestone. *Ceramics Silikaty*, 50(3):167.
[28] El-Didamony, H., El-Rahman, E. A., Osman, R. M. (2012). Fire resistance of fired clay bricks–fly ash composite cement pastes. *Ceramics International*, 38(1):201–209.
[29] Lilkov, V., Rostovsky, I., Petrov, O., Tzvetanova, Y., Savov, P. (2014). Long term study of hardened cement pastes containing silica fume and fly ash. *Construction and Building Materials*, 60:48–56.
[30] Tanyildizi, H., Coskun, A. (2008). The effect of high temperature on compressive strength and splitting tensile strength of structural lightweight concrete containing fly ash. *Construction and Building Materials*, 22(11):2269–2275.
[31] Donatello, S., Tyrer, M., Cheeseman, C. R. (2010). Comparison of test methods to assess pozzolanic activity. *Cement and Concrete Composites*, 32(2):121–127.
[32] Nasser, K. W., Marzouk, H. M. (1979). Properties of mass concrete containing fly ash at high temperatures. *ACI Journal Proceedings*, 76(4):537–550.
[33] Shaw, S., Henderson, C. M. B., Komanschek, B. U. (2000). Dehydration/recrystallization mechanisms, energetics, and kinetics of hydrated calcium silicate minerals: an in situ TGA/DSC and synchrotron radiation SAXS/WAXS study. *Chemical Geology*, 167(1–2):141–159.
[34] Linh, T. H. (2014). *Networks and Their Applications in Signal Processing*. Hanoi University of Science and Technology Publisher, Vietnam.